IOP Publishing Measurement Science and Technology
Journal **XX** (XXXX) XXXXXX https://doi.org/XXXX/XXXX

Perspective on the Development and Application of Light-Field Cameras in Flow Diagnostics

Zu Puayen Tan[1] and Brian S. Thurow[2]

[1] Department of Mechanical Engineering, National Yang Ming Chiao Tung University, Hsinchu City, Taiwan
[2] Department of Aerospace Engineering, Auburn University, Auburn, U.S.A.

E-mail: tanzu@nctu.edu.tw , thurow@auburn.edu

Received xxxxxx
Accepted for publication xxxxxx
Published xxxxxx

Abstract

Multi-camera flow diagnostics have made large gains in recent years in the field of three-dimensional and multi-physics measurements. However, cost, complexity and optical access pose challenges that place multi-camera techniques out of reach for many labs. In that context, light-field (LF) imaging represents an alternative approach that can potentially alleviate some of these challenges. LF flow diagnostics is a branch of measurement techniques introduced within the last decade that are based on a plenoptic camera's unique ability to capture three-dimensional and multi-spectral data via a single objective lens and image sensor. Thus far, LF flow diagnostics have successfully achieved significant camera-reduction alongside other performance improvements in 3D flow velocimetry, 3D particle tracking, 3D scalar-field tomography, micro-fluidic velocimetry and multi-spectral imaging, as well as early demonstrations of single-camera multi-physics measurements for applications such as 3D fluid-structure interactions. Here, we discuss the state of development in LF flow diagnostics, highlight on-going challenges, and project potential advancements in the near future.

Keywords: light-field, plenoptic, microlens array, 3D flow diagnostics, particle image velocimetry, tomographic PIV, plenoptic PIV, particle tracking velocimetry, 3D-PTV, light-field microscopy, scalar-field tomography, 3D background-oriented schlieren, multi-spectral imaging

1. Introduction

Modern advances in fluid dynamics require understanding of increasingly three-dimensional (3D), unsteady and multi-physics phenomena, ranging from 3D fluid-structure interactions (FSI) in soft robotics to the aerothermodynamics of hypersonic vehicles. Image-based flow diagnostics continue to be indispensable, as more complex computational models in increasingly extreme environments require on-going empirical validations. However, the progress and application of advanced image-based flow diagnostics are currently impeded by the paradigm of increasing camera-count, where capturing more complex flows require increasingly more costly scientific-grade cameras per experiment.

IOP Publishing Measurement Science and Technology
Journal **XX** (XXXX) XXXXXX https://doi.org/XXXX/XXXX

For example, as Fig. 1 illustrates, early particle image velocimetry (PIV) experiments employed only one camera for 2D two-component (2C) measurements. Later, stereo-PIV extended the technique to 2D-3C by adding a second camera, while tomographic PIV (tomo-PIV) and 3D particle tracking velocimetry (3D-PTV) used three to four *high-speed* cameras to obtain 3D-3C time-resolved velocity-fields [1]. Numerous contemporary research have also begun to combine tomo-PIV/3D-PTV with simultaneous measurements of additional physics using setups with five or more cameras; e.g. FSI [2,3] and simultaneous velocimetry with flame-front visualization [4,5]. This paradigm can present significant challenges for many applications due to:

i. Inflating costs of experiments.
ii. Increasing alignment complexity and sensitivity.
iii. Expanding footprint and optical access requirement that are incompatible with facilities such as combustion rigs, hypersonic wind tunnels or small biological samples.
iv. And finally, the more technical disadvantage of depth-of-field (DOF) versus light-sensitivity tradeoff, where reduction of lens aperture in already light-starved volumetric measurement is often necessary to gain sufficiently large DOF to encompass the volume.

Breaking the existing paradigm is therefore critical in order for modern image-based flow diagnostics to be applied to an even broader set of problems that might benefit from these advanced measurement techniques.

Attempts to break the paradigm of increasing camera-count thus far include the view-splitter ("quadscope") [6,7] and fiber-optic techniques [8] that combine multiple perspective-views onto a single sensor; the MiniShaker [9] and co-axial volumetric PIV [10] that pack multiple small cameras into a compact camera head; as well as defocusing PIV [11], digital holographic PIV [12] and color-coded PIV [13] that leverage aperture-related or non-perspective-views physics to generate 3D data. In addition to these techniques, a unique branch of camera-reduction strategies has emerged in recent years based on the novel plenoptic (aka. light-field, LF) imaging principle. Unlike conventional cameras, plenoptic imagers employ a microlens array (MLA) to capture 4D light-ray data within a single shot via a single objective lens, following which, a multiplicity of images with varying perspectives, focal points and extended DOF can be rendered. These powerful capabilities have been successfully leveraged to achieve 3D flow velocimetry, fragment/particle-tracking, microscopy, scalar-field tomography, and hyperspectral measurements. Here, we review progress in the nascent field of plenoptic flow diagnostics and provide perspectives on likely future developments.

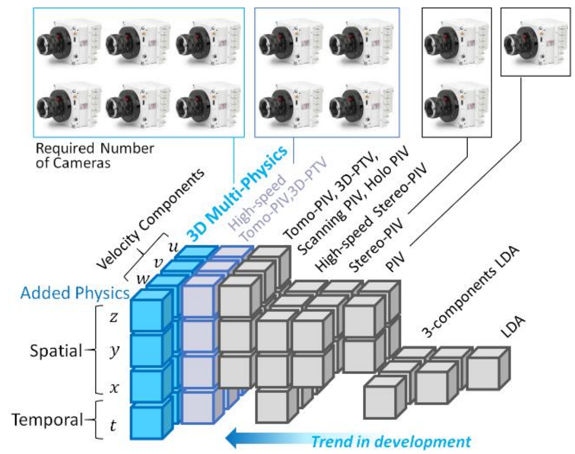

Fig. 1 The curse of camera-count. Based on: [1]

2. Principles and Hardware of Light-Field Imaging

LF imaging begins with the treatment of light as 4D rays in 3D space, each ray having a 2D spatial coordinate (s,t) on a datum plane, as well as 2D directional coordinate (u,v) on a parallel plane at another depth z. In the reference frame of a camera (Fig. 2), (u,v) is mapped on the main-lens aperture while (s,t) is mapped to the sensor-plane. Thus the (x,y,z) position of a light-source relative to the camera can be computed if the LF coordinates of its rays are known. A regular camera does not capture LF data because the act of focusing collapses (u,v) information to a point, as illustrated in Fig. 2. Plenoptic cameras preserve (u,v) by imaging the aperture plane (u,v information) at discrete locations along the sensor using the MLA.

Two distinct architectures of plenoptic cameras exist: the original plenoptic 1.0 camera (aka. unfocused plenoptic) [14,15] and the later plenoptic 2.0 (aka. focused plenoptic) camera [16–21]. Plenoptic 1.0 and 2.0 differ in the positioning of their MLA (Fig. 2) which subsequently affects the sampling of LF information (Fig. 3). The plenoptic 1.0's MLA coincides with the main-lens' nominal

IOP Publishing Measurement Science and Technology
Journal **XX** (XXXX) XXXXXX https://doi.org/XXXX/XXXX

image-plane, while the sensor is one microlens focal-length behind the MLA. As such, rays focused on the nominal image-plane are neatly re-expanded into unfocused circular sub-images on the sensor occupying the same footprint as a microlens diameter. In contrast, plenoptic 2.0 has an MLA that is focused on the nominal image-plane, such that each microlens acts as a mini relay-lens conveying cropped, overlapping versions of the full image onto the sensor. Example of plenoptic 1.0 and 2.0's raw images are given in [16]. Consequently, as Fig. 3 shows, a given microlens discretely samples multiple (u, v) at a fixed (s, t) coordinate in plenoptic 1.0, whereas in plenoptic 2.0 a microlens samples a range of (s, t) and (u, v) whose values are coupled. Typically, plenoptic 2.0's pixels are distributed more densely in (s, t) and less in (u, v) relative to 1.0. Notably, the pixel distribution is fixed to hardware for 1.0, but can be easily re-optimized via shifting the MLA in 2.0- a key advantage of the latter.

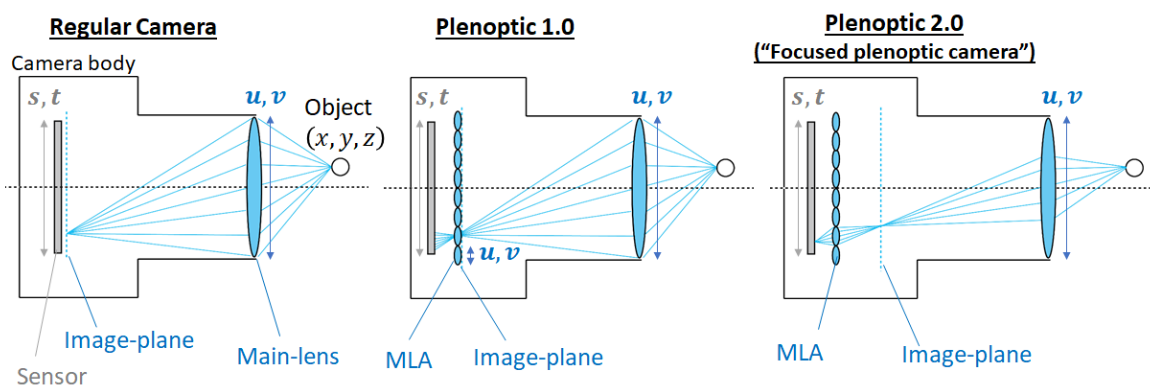

Fig. 2 Comparison of a conventional versus plenoptic 1.0 and 2.0 cameras.

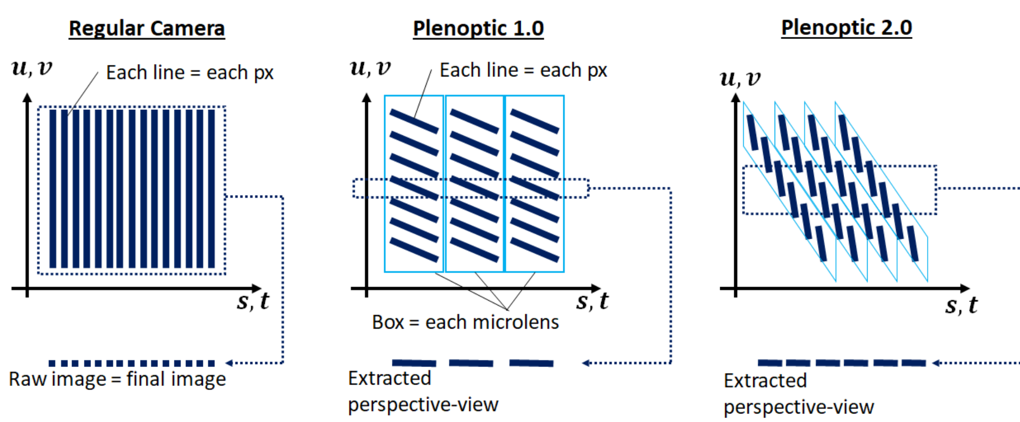

Fig. 3 Comparison of recorded information between conventional versus plenoptic 1.0 and 2.0 cameras. The schematic illustrates sampling for focal-plane objects, and is sheared when rays originate from off-focal planes.

The raw images of both plenoptic architectures must be decoded to provide meaningful viewing. Two commonly used decoding methods are as follows:

1. *Perspective-view generation:* a slice of pixels is extracted out of Fig. 3's diagram at the desired perspective angle (u, v). Physically this represents extracting a single pixel from behind each microlens at a constant location and assembling them to form an image. A perspective-view has unusually large DOF for the given main-lens setup (more details later), while changing the extraction (u, v) shifts the viewer's perspective.
2. *Refocusing:* an image with regular (thin) DOF is generated by integrating across (u, v) in Fig. 3's diagram. Direct integration leads to an image focused on the main-lens' nominal focal-plane.

IOP Publishing Measurement Science and Technology
Journal **XX** (XXXX) XXXXXX https://doi.org/XXXX/XXXX

Conversely, if the sample points in Fig. 3 are sheared prior to integration (representing propagation of rays in z), the image can be synthetically refocused to different depths.

Due to the different pixel distributions, perspective-views with more precise (u, v) can be obtained in plenoptic 1.0, albeit at lower spatial (s, t) resolution than 2.0. Similarly, refocused images with higher spatial resolutions can be obtained from 2.0. However, artifact-free images are difficult to obtain from 2.0 as a raw pixel straddles a wider range of (u, v). Additional procedures to reduce artifacts often must be implemented and typically include either an explicit or implicit determination of an object's depth within the scene, which can present challenges in more complex 3D scenes. Aside from resolution trade-offs, plenoptic 1.0 and 2.0 also offer different conveniences from a workflow viewpoint: the decoupled (s, t) and (u, v) in 1.0 is suitable to applications requiring high (u, v) resolution such as hyperspectral imaging (discussed later), while the ability of 2.0 to re-optimize (s, t) versus (u, v) precisions by shifting the MLA is highly desirable for applications such as PIV albeit with a significant increase in complexity of the associated image processing scheme. For brevity, further details on architectures and decoding are left to [20,22,23].

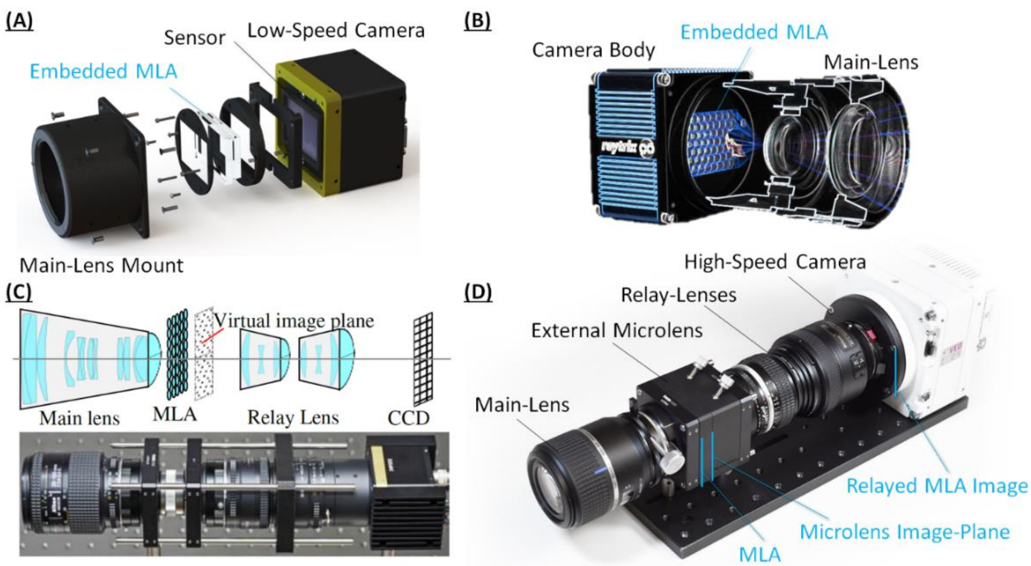

Fig. 4 Examples of plenoptic hardware used in fluid dynamics research: (A) a modified low-speed camera with embedded MLA for plenoptic 1.0 imaging. (B) Raytrix's commercial plenoptic 2.0 camera. [24] (C) Relayed MLA to support rapid prototyping. [25] (D) Relayed MLA used on a high-speed camera. [26,27]

Finally, two approaches are used to physically implement plenoptic imaging, neither of which is trivial as the MLA's miniscule focal length requires tenths of a millimeter or smaller tolerances. In matured research cameras such as Fig. 4A or commercial cameras such as Lytro and Raytrix devices (Fig. 4B), the camera sensor is removed of its glass cover and the MLA embedded directly in a factory clean room. Embedded MLA provides superior optical performance and compactness, but is less feasible for rapid prototyping or flexibly retrofitting high-cost systems like high-speed cameras and intensifiers. The latter requirement prompted a second type of design where the MLA is located externally and has its image relayed via lenses onto the sensor, thereby requiring no modification to the sensor body (see Fig. 4C-D) [14,25–30]. This design is especially demanding of the relay lenses' field flatness and aperture, which must accommodate the MLA's focal length tolerance and divergent ray angles.

In the next few years, we expect improvements in sensors and MLA fabrication to gradually enable higher resolution and cheaper plenoptic cameras. Additionally, several innovations on the horizon are also expected to reform plenoptic imaging. These include but are not limited to: (i) Actively-driven MLA and associated algorithms that seamlessly

IOP Publishing Measurement Science and Technology
Journal **XX** (XXXX) XXXXXX https://doi.org/XXXX/XXXX

transition between plenoptic 1.0 and 2.0 to provide on-the-fly optimization for varying experimental needs. (ii) Better image decoding to improve resolutions and reduce image artifacts of rendered plenoptic images for a given hardware design; e.g. super-resolution by conventional [31] or deep-learning methods. And (iii) LF imaging based on camera array instead of MLA such as the synthetic aperture PIV technique [32], especially via the use of cheap but increasingly capable smartphone camera sensors- most notably in the footsteps of Pelican [33] and Light's multi-camera LF-imaging phones [34].

3. Application to Flow Velocimetry

"Plenoptic-PIV" forms the core of LF flow diagnostics with successful applications in the studies of small marine animals [35] (Fig. 5A, Fig. 6A), compressor linear cascade [36] (Fig. 5B, Fig. 6B), birds and maneuvering wings [37], riverbed boundary-layer [38], shock-boundary layer interactions [39,40] (Fig. 5C, Fig. 6C), thin liquid film [41], rotating helicopter blade [42] (Fig. 5D, Fig. 6D), transcatheter heart valves [43] and numerous others. In Fig. 5-Fig. 6's examples, constraints on optical access and depth of volume would have made a multi-camera system very challenging to implement.

As with many other plenoptic flow diagnostic techniques introduced below, the earliest 3D velocimetry via plenoptic-PIV was achieved by leveraging the camera's refocusing capability. Image of a particle-field was refocused to planes at discrete depths (called a "focal stack"), after which sharpness-detection or intensity-based segmentation attempts to localize particles to their corresponding depth based on defocus blurring. This technique is not robust and has relatively low depth resolution.

The current realization of plenoptic-PIV with improved robustness and resolution adopts a similar workflow as tomo-PIV (see Fig. 7). The raw plenoptic image of the particle field is first decoded into a stack of perspective-views at discrete (u, v). A virtual particle volume is then reconstructed by operating on the perspective-views with a tomographic algorithm such as the standard Multiplicative Algebraic Reconstruction Technique (MART):

$$E(x_j, y_j, z_j)^{k+1} = E(x_j, y_j, z_j)^k \left[\frac{I(s_i, t_i)}{\sum_{j \in N_i} w_{i,j} E(x_j, y_j, z_j)^k} \right]^{\mu w_{i,j}}$$

where E denotes voxel intensity at (x_j, y_j, z_j) on the k^{th} iteration; I denotes intensity of pixel at (s_i, t_i); and summation in the denominator is carried out for the set of voxels N_i in the line-of-sight of pixel $I(s_i, t_i)$; while, μ is the iteration's relaxation factor. Critically, $w_{i,j}$ is a weighting factor that relates the projection of a 2D pixel in a perspective-view to 3D voxels, and is closely related to 3D calibration of the camera system. After reconstruction, two sequential volumes are cross-correlated to produce a 3D velocity-field. In this respect, the only key distinction between plenoptic-PIV and tomo-PIV is the nature of the perspective-views. In plenoptic-PIV, upwards to 100 perspective-views can be obtained from a single raw image, but only with a parallax baseline as wide as the main-lens' aperture, which fundamentally limits depth resolution.

For more details, early development of the plenoptic-PIV technique is described by Lynch et al. [44], while subsequent improvements are covered in [45–47]. Like tomo-PIV, numerous alternatives to MART were proposed to improve accuracy or expedite convergence, including dense ray-tracing reconstruction [48], filtered refocusing [49], deconvolution [50] and expectation-maximization with summed line-of-sight estimation [51]. Expediting is significant for plenoptic-PIV due to the computational cost of iterating through a large number of perspective-views compared to just four in tomo-PIV. Concurrent studies are also exploring whether under-sampling the available perspective-views but maintaining total parallax baseline will reduce computation without adverse effects on reconstruction.

IOP Publishing Measurement Science and Technology
Journal **XX** (XXXX) XXXXXX https://doi.org/XXXX/XXXX

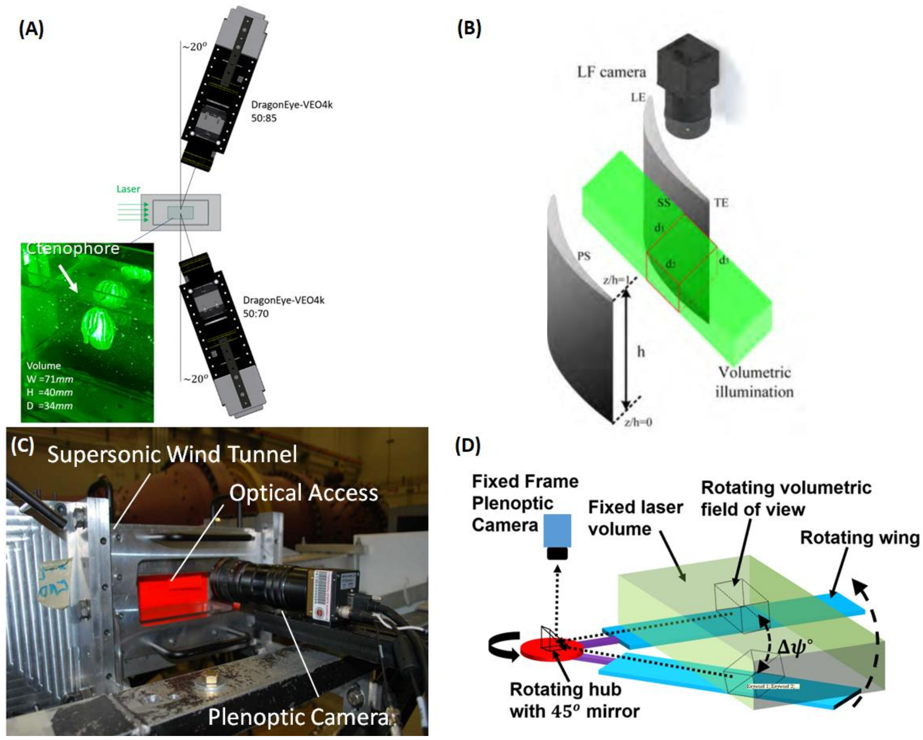

Fig. 5 Application of plenoptic-PIV in the measurements of (A) ctenophore hydrodynamic [35], (B) flow within a compressor linear cascade [36], (C) supersonic swept-fin [40], and (D)leading-edge vortex dynamic about a rotating frame-of-reference [42].

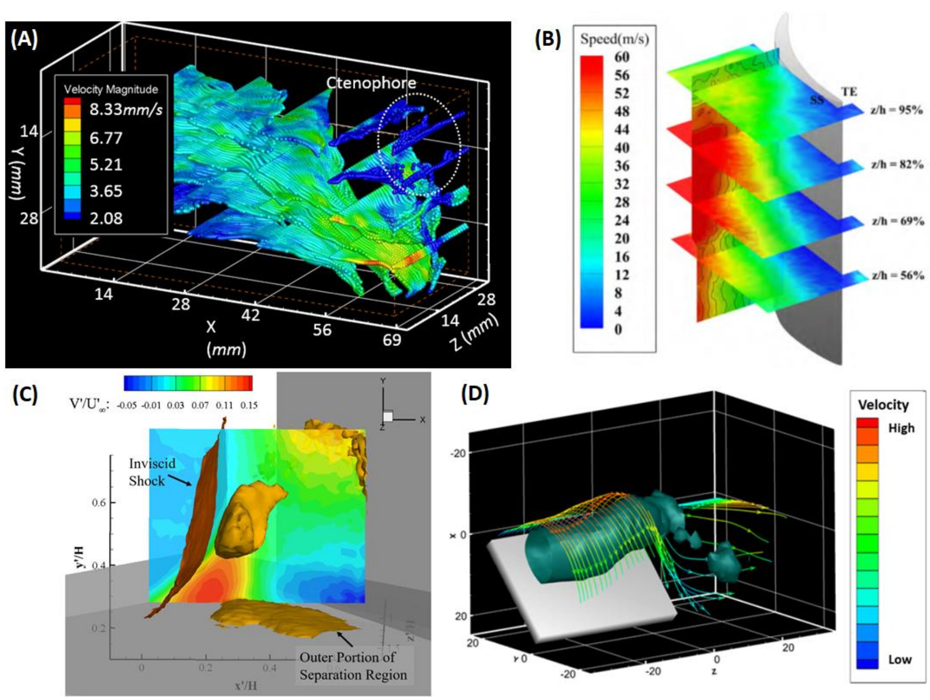

Fig. 6 Results corresponding to experiments and references (A-D) above, respectively.

IOP Publishing Measurement Science and Technology
Journal **XX** (XXXX) XXXXXX https://doi.org/XXXX/XXXX

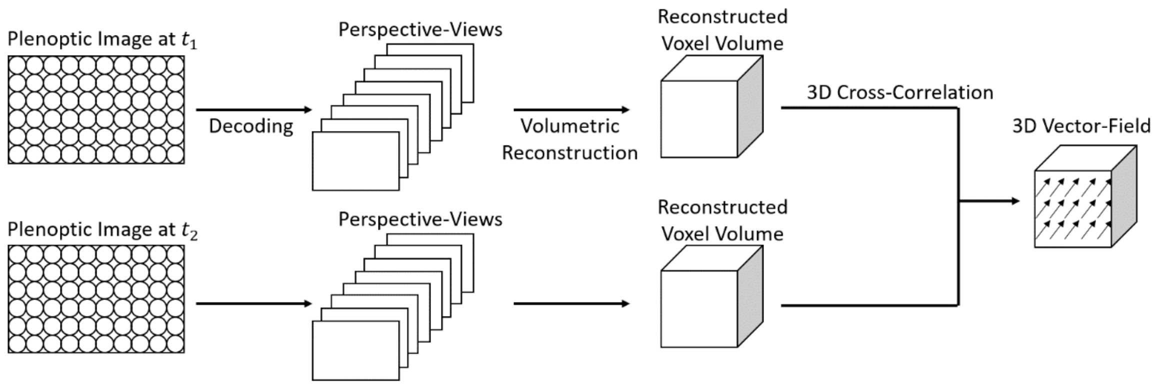

Fig. 7 Workflow of plenoptic PIV.

As noted above, $w_{i,j}$ establishes the relation between the image and 3D world and is foundational to 3D reconstruction. The standard practice in four-camera tomo-PIV involves generating a separate pinhole or polynomial calibration model for each camera, from which $w_{i,j}$ is calculated. However, the availability of ~100 perspective-views in plenoptic-PIV and the possibility of dynamically sampling *different* sets of perspective-views from the same image makes tomo-PIV's approach impractical. An early method of plenoptic calibration developed by Thomason et al. [52] in 2014 employed a root-mean-square procedure to estimate the positions of the sensor, MLA and main-lens, after which a geometrical model relates image to 3D world. In 2018, Hall et al. [53,54] developed a more robust and flexible third-order polynomial calibration scheme for plenoptic 1.0 cameras, where the image-to-world mapping of all possible perspectives are fitted with two 3rd-order polynomials, P_s and P_t, for the two orthogonal sensor directions:

$$s = P_s(x, y, z, u, v)$$
$$t = P_t(x, y, z, u, v)$$

Hall et al.'s scheme has the advantage of storing only a small set of polynomial coefficients, but additional constraints are required to translate the calibration scheme into $w_{i,j}$; e.g. the assumption of comparable size between voxels and microlens pitch. Early efforts to pre-compute and store the entire $w_{i,j}$ matrix quickly exceeded a typical workstation's memory. Consequently, a model that translates P_s, P_t to $w_{i,j}$ is now used to calculate weighting on-the-fly. Dynamic sampling of (u, v) is allowed in this method, but the polynomial has the disadvantage of being uni-directional where solving x, y, z based on (s, t, u, v) is computationally difficult. Ongoing work by the authors' groups suggests that re-fragmenting the polynomial into separate calibrations for each (u, v) may significantly improve accuracy, though this once again prevents dynamic (u, v) sampling without, say, interpolating coefficients.

In 2019, Shi et al. [55] proposed an alternative scheme, which models ray-propagation through the plenoptic camera using thin-lens model with higher order corrections for complex lens distortion and MLA displacement. Notably, the thin-lens formulation is written in terms of the position and diameter of the circle-of-confusion that a point-source produces on a plenoptic image. Calibration then involves imaging a set of point-sources at various positions to establish the camera parameters. The computation of $w_{i,j}$ is subsequently based on Monte-Carlo tracing of 100 rays through the system using the camera parameters. The method was further developed in 2020 [56] to incorporate the concept of "plenoptic disk" (similar to circle-of-confusion).

While $w_{i,j}$ is often used in the direction of mapping 3D voxel to 2D pixel, Cao et al. [51] recently developed a new scheme that employs the reversed tracing direction for a plenoptic 2.0 camera. The main motivation being that reversed-tracing connects one pixel to multiple voxels at once, thereby reducing to total number of ray-tracing computations. In another ongoing development, a unique variant of Hall et al.'s polynomial calibration was developed by Gururaj et al. [42]. Driven by engineering needs, their plenoptic camera was aligned on the hub of a rotating helicopter blade (Fig. 5D), which has a 45^o mirror that reflected the view onto the blade. The setup allows for 3D PIV on a

IOP Publishing Measurement Science and Technology
Journal **XX** (XXXX) XXXXXX https://doi.org/XXXX/XXXX

rotating frame-of-reference that was previously untenable with multi-camera tomo-PIV. A rotating version of the polynomial calibration was thus devised for this application. In addition to the mentioned works, we anticipate that near-future development will likely drive towards increasingly automatic and physically-informed calibration schemes, as well as adoption of higher-order corrections such as tomo-PIV/3D-PTV's volumetric self-calibration algorithm [57].

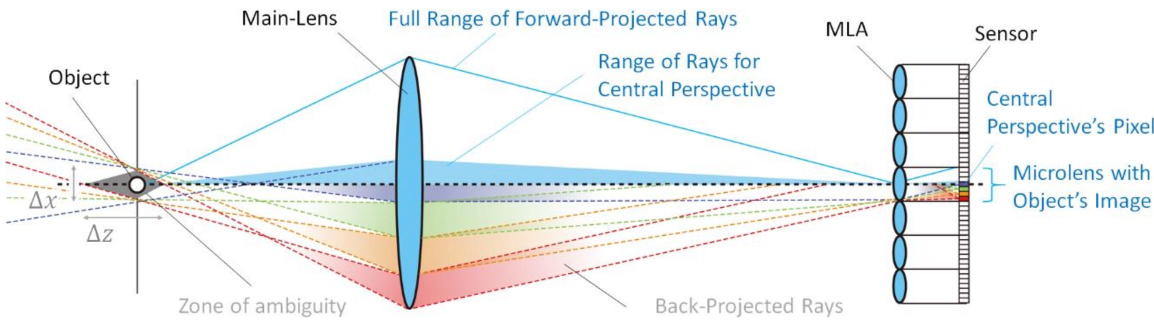

Fig. 8 Principles behind extended-DOF (top) and particle elongation (bottom) in plenoptic-PIV.

It is worth briefly discussing an additional strength and limitation of plenoptic-PIV: DOF and particle-elongation, respectively. Multiple cameras must share a common DOF encompassing the measured volume in tomo-PIV. As discussed in [58], DOF for an imaging system is given by:

$$DOF = 2\frac{d_{aper}c_o}{d_{aper}^2 + c_o^2} z_{nominal}$$

Where d_{aper} is the imaging aperture diameter, c_o is the allowable circle-of-confusion's size in object-space (e.g. pixel pitch), and $z_{nominal}$ is the nominal focal-plane's distance from the aperture. For conventional imaging, d_{aper} corresponds to the main-lens' aperture diameter. For plenoptic camera, however, Fig. 8 shows that a perspective-view is formed by extracting a pixel behind a microlens. The pixel contains a small range of (u, v) and physically only gathers rays from a fraction of d_{aper} (see "Range of Rays for Central Perspective"). This has the effect of rendering the equivalent aperture as:

$$d_{aper,equivalent} = \frac{d_{aper}}{pxpm}$$

Where $pxpm$ is the number of pixels per microlens. Consequently, DOF is significantly increased in perspective-view. DOF in refocused images remain unchanged and is dependent on the full aperture, which is typically quite large in plenoptic cameras (order f/2 – f/4). Notably, the reduction in effective aperture is perfectly balanced by the reduction in perspective-view's resolution, which effectively increases the "pixel" size. Hence, a perspective-view pixel has the same signal-to-noise ratio as a conventional camera's pixel, *but* at a much lower total pixel count, thus only using a fraction of the collected light. If all perspective-views participate in volumetric reconstruction, the contribution from all collected light is naturally regained, without losing the benefit of extended DOF.

A key limitation of plenoptic-PIV (and any plenoptic 3D measurements) is the limited parallax angle straddled by its single main-lens. As shown in bottom of Fig. 8, an on-axis point source at the nominal focal-plane fills all pixels under the center microlens. If rays are projected backwards from these pixels, finite rays of light-cones are formed (purple, green, orange and red cones in Fig. 8). All rays within a cone will fall on the same pixel; hence, a cone demarks a zone of ray ambiguity. The intersections of all cones form a diamond-shaped region around the real point source, within which we cannot determine the point source's true location with certainty. Hence, the width of the "diamond" represents the system's lateral resolution (Δx) and its length the depth resolution (Δz). Notably, Δx and Δz are both depth-dependent.

A tomographic algorithm such as MART would thus reconstruct a circular flow particle as an elongated "diamond" filling the zone of ambiguity. Elongation grows worse with particle size and distance between camera and object. Using commercial lenses where the F-number is generally limited to 1.2, plenoptic cameras are usually only suitable for volumes with lateral dimension smaller than the order of 100 mm before elongation begins to severely impact PIV accuracy. Details on the accuracy of plenoptic cameras in PIV application are

IOP Publishing Measurement Science and Technology
Journal **XX** (XXXX) XXXXXX https://doi.org/XXXX/XXXX

given by [58–60], while [61] directly compares a single-camera plenoptic-PIV against four-camera tomo-PIV. A direct solution to elongation involves adding a second plenoptic camera at 70-90^o to the first, which drastically reduces the zone of ambiguity to the intersection region of both cameras' "diamonds" [35,58,62,63].

Future developments of plenoptic-PIV will naturally benefit from continued accelerations in reconstruction, either through algorithmic improvements or optimizing the number of required perspectives. Reconstruction accuracy is also expected to increase with improvements in calibration scheme, higher-resolution image-decoding and incorporation of prior knowledge into reconstruction. Advanced cross-correlation algorithms with optimized kernels [64] are also in development to reduce to impact of elongations and other reconstruction artifacts.

4. Application to 3D Tracking

The development of plenoptic-PTV and 3D-tracking can be traced to three motivators: (i) it is an extension of plenoptic cameras' earliest application in depth-sensing [14], (ii) under many scenarios 3D-PTV require less compute and storage costs than tomographic reconstruction, and (iii) the Lagrangian approach localizes particles to a specific value in lieu of an elongated group of voxels in plenoptic-PIV (though a higher Δz uncertainty could still manifest). Like plenoptic-PIV the earliest approach to 3D tracking for both plenoptic 1.0 and 2.0 involve creating a focal-stack, whereby depth localization of objects or particles is performed through determination of the focal slice with the sharpest image edges (see Fig. 9A) [65,66]. However, this approach is often slow and has limited resolution in z.

Present approaches to 3D tracking differ substantially between plenoptic 1.0 and 2.0 (see Fig. 10). In the former, the raw image is first decoded into perspective-views. Image segmentation then tags particles/objects of interest with associated (s, t, u, v) coordinates. Next, coordinates belonging to the same object appearing across multiple perspective-views are found, similar to the "correspondence problem" in multi-camera 3D-PTV or stereo-photogrammetry, except in this case ~100 perspectives exist. Finally, the object's (x, y, z) position is triangulated by projecting it rays to where they intersect and originated based on (s, t, u, v), with the associated camera calibration in the loop.

As shown in Fig. 10A, an early K-means clustering approach developed by Hall et al. [54,67] for large fragment tracking lays out all identified object centroids on a 2D (s, t) plot. Each point still retains its (u, v) identity. A K-means clustering algorithm performed on the 2D space then identifies sets of centroids belonging to the same object. Finally, (x, y, z) is solved based on the clustered (s, t, u, v) sets. Though precise, K-means clustering in 2D was not robust for flow velocimetry with high particle densities. The approach is more applicable to large fragment tracking, such as shown in Fig. 9B.

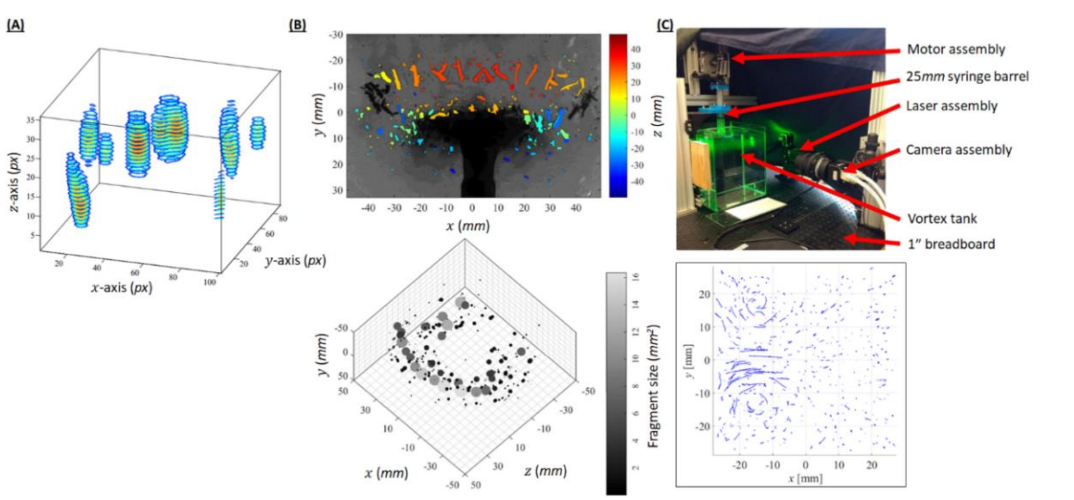

Fig. 9 (A) Example of 3D tracking via focal-stack [66]. (B) Example of explosive fragment tracking and sizing by K-means clustering of plenoptic 1.0 perspective-views [67]. (C) Vortex ring 3D PTV via plenoptic 2.0's ETC method [68].

IOP Publishing Measurement Science and Technology
Journal **XX** (XXXX) XXXXXX https://doi.org/XXXX/XXXX

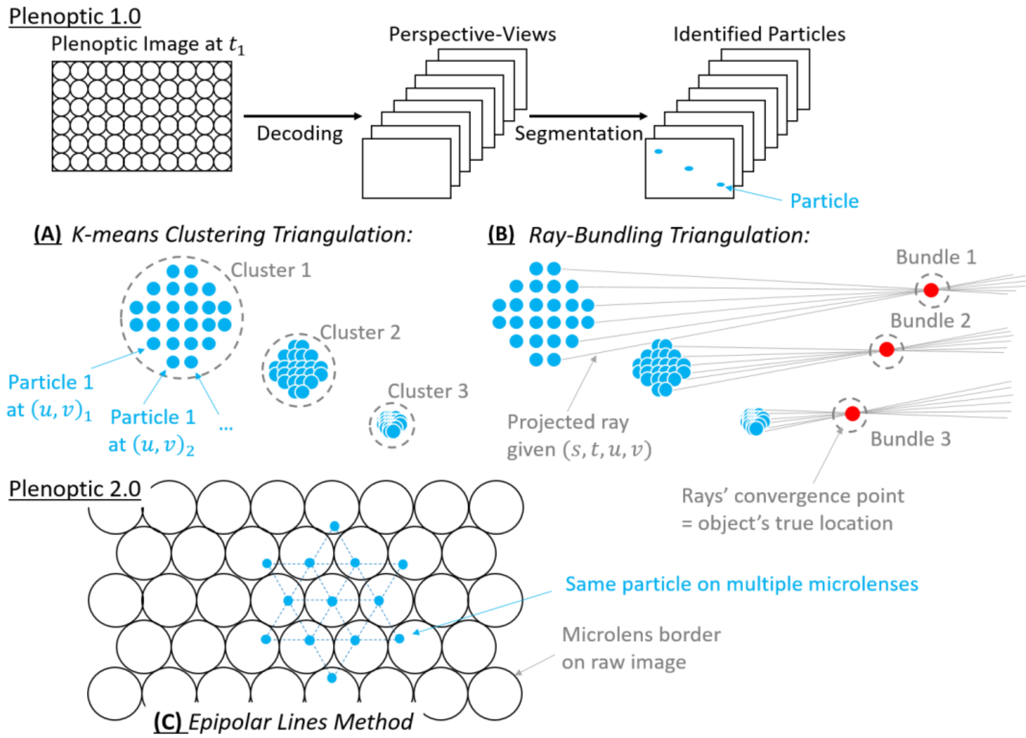

Fig. 10 Different approaches to plenoptic PTV and particle-tracking: (A) K-means 2D clustering and (B) "Ray-bundling" 3D clustering for plenoptic 1.0, (C) Epipolar Triangular Connections for plenoptic 2.0.

In response, Clifford et al. [69] developed the "Ray-Bundling" method that extended K-means clustering into 3D space by treating each (s,t,u,v) as a projected ray. The underlying assumption being that the plenoptic camera samples hourglass-shaped bundles of rays from every particle (Fig. 10B). Expansion to 3D space makes the projected rays relatively sparse, and robust clustering can be performed to identify bundles based on their minimum crossing distances. Clifford et al. [69] successfully demonstrated the Ray-Bundling algorithm at 3D-PTV levels of particle densities. And, though computational cost scales with the number of particles, the aggregate computations for practical experiments remain lower than plenoptic-PIV. A direct comparison of accuracies for MART-reconstruction and tracking remains to be done. Preliminary efforts by [69] suggest Ray-Bundling result in lower errors than MART in all directions, though errors in the z-axis remain up to z5 times higher than xy-axes.

PTV via plenoptic 2.0 cameras uses a distinct method (Fig. 10C) that is more akin to multi-camera 3D-PTV's epipolar line approach. The plenoptic 2.0 approach proposed by [68] called "Epipolar Triangular Connections (ETC)" method leverages its in-focus raw image to bypass perspective-view decoding. Instead, particle segmentation occurs directly on the raw plenoptic image. The correspondence problem is solved beginning with an identified particle, followed by extension of epipolar lines outwards from this particle to adjacent microlenses, which effectively act as neighboring micro-cameras. Corresponding images of the particle are sought in adjacent microlenses, and if found the epipolar lines are extended outwards again, until a diameter corresponding to the maximum CoC in the measured volume is reached. The physical particle location is then found by triangulating from the found set of (s,t,u,v). This approach has the advantage of bypassing image-decoding, which not only expedites computation but also avoids any decoding artifacts, especially those associated with the perspective-view's low resolution (a major impediment to segmenting dense particle fields in plenoptic 1.0). Example of applying the ETC method to measure a vortex ring flow is shown in Fig. 9C. At the point of writing the method is still undergoing refinement.

IOP Publishing Measurement Science and Technology
Journal **XX** (XXXX) XXXXXX https://doi.org/XXXX/XXXX

Overall, plenoptic-PTV via both 1.0 and 2.0 approaches are still in their infancy relative to multi-camera 3D-PTV. In addition to gradual improvements in accuracy and computation costs, we expect the next step in development of plenoptic-PTV to include integration of proven advanced 3D-PTV algorithms such as iterative particle reconstruction (IPR) and Shake-the-Box (STB), as well as customization of these algorithms to exploit plenoptic cameras' perspective redundancy. We also note that plenoptic-PTV and 3D tracking is conceptually very similar to plenoptic depth estimation, which contains a vast literature partially covered in [22]. The depth estimation literature includes Adelson & Wang's landmark paper [14] on plenoptic 1.0 camera, as well as many plenoptic 2.0 algorithms [17,20] where depth calculation from disparity map is integrated into the image-decoding workflow. The implications of these algorithms have not been fully explored for fluid diagnostics and further work is required.

5. Application to Microscopy

The application of plenoptic cameras in micro-fluidic measurements is primarily motivated by the lack of optical access. Many biological processes are dynamic and 3D, but placement of multiple microscope objective lenses and illuminators around a microscopic subject is inherently difficult [70]. Additionally, microscope objective lenses have very shallow DOF, while many of them are also object-space telecentric, thus offering no perspective parallax when translated relative to the subject. Thus, a plenoptic camera's ability to refocus and shift perspective within a single image is highly sought after in microscopy.

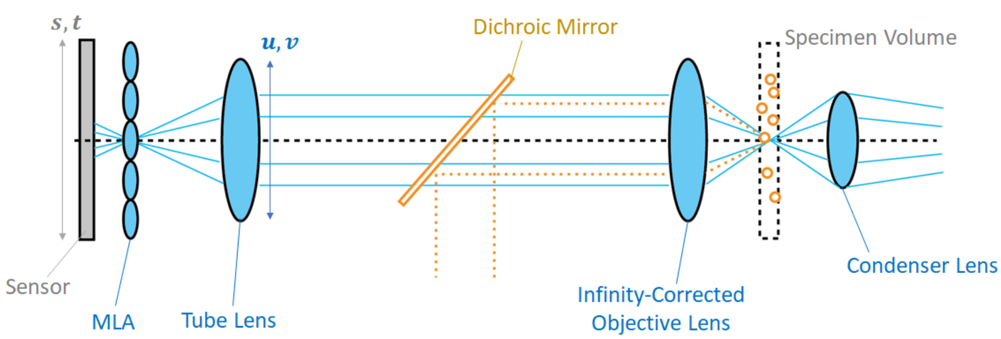

Fig. 11 Typical architecture of plenoptic microscope.

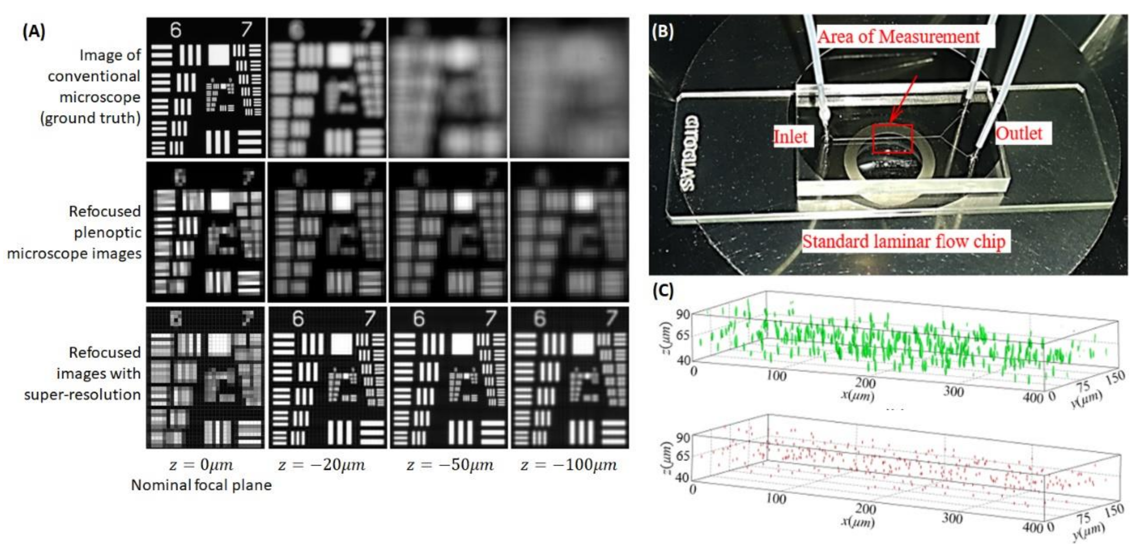

Fig. 12 (A) Plenoptic microscope images refocused to a translating target's corresponding planes, without and with super-resolution, as compared to a non-refocusing conventional microscope image [71]. (B) Example of plenoptic micro-PIV on a flow chip. (C) 3D particle reconstruction (green) from the flow-chip, with the additional step of particle centroid-finding (red) prior to cross-correlation [30].

IOP Publishing Measurement Science and Technology
Journal **XX** (XXXX) XXXXXX https://doi.org/XXXX/XXXX

A typical plenoptic microscope's layout is schematically illustrated in Fig. 11 [30,66,72–74], comprising of a condenser lens for focusing illumination onto the subject, an infinity-corrected objective lens and a tube lens. The MLA is placed at the tube lens' image-plane, followed by the sensor at its usual placement behind the MLA. (s, t) and (u, v) are mapped in the typical manner. For micro-PIV applications where particles are seeded into the specimen volume, illumination can also be introduced along the optical path via an angled dichroic mirror to elicit back-scattering signals from particles.

Though the standard plenoptic refocusing and perspective-view procedures apply to microscopy, wave optics must be considered for accuracy due to diffraction at this scale. Compared to macro-scale volumetric reconstruction with tomography equations, the microscopy community has a longer history with the deconvolution approach tracing back to the use of non-plenoptic cameras [71]. The original approach consists of focusing a conventional camera on a microscopic subject, and then physically translating the subject in depth to generate a focal-stack. Deconvolving the focal-stack with the system's point spread function (PSF), which is conveniently shift-invariant for a telecentric microscope objective, then reconstructs the subject volume. Notably, Levoy et al. [72] showed that deconvolution is fundamentally equivalent to limited-angle tomographic reconstruction.

Acquisition of focal-stack via physical translation is not possible for highly dynamic subjects; thus, plenoptic microscopy offers a valuable alternative where the light-field is instantaneously captured, and a focal-stack can be synthetically generated. In early implementation by Levoy et al. [72], the plenoptic system's PSF was empirically determined by imaging a sub-pixel fluorescent bead to approximate a point-source; later, Broxton et al. [71] proposed a more comprehensive model that accounts for plenoptic systems' non-uniform sampling of a scene at different depths and, consequently, its shift-variant PSF. Additionally, as Fig. 12A shows, using super-resolution procedures that exploit the system's non-uniform sampling pattern, Broxton et al. [71] was also able to gain resolutions that were 8 times higher than a naïve 1:1 (s, t)-(u, v) tradeoff would otherwise offer.

More recent developments in plenoptic microscopy include the concept of selective volume illumination (SVM), which found that 3D reconstruction and refocusing have lower artifacts when the illumination is confined to the depths of interest in lieu of a back-light that permeates the volume [70,75]. On the other hand, Levoy et al. [73] proposed that in addition to imaging, a second MLA can be installed and operated in "reverse" as an illuminator to achieve depth-modulated illumination. Finally, successful demonstrations of velocimetry on the micro scale include [30,74] for PIV (see Fig. 12B-C) and [66] for PTV. Given its vast potentials, plenoptic microscopy is developing into a field of its own. The future of plenoptic flow diagnostics will likely benefit from adopting unique techniques developed from the general plenoptic microscopy community.

6. Application to Scalar-Field Measurements

The use of plenoptic cameras for 3D scalar-field measurements involves reconstruction of a 3D luminescent field such as flame or fluorescing flow [76–81], and in some instances, further specialization into simultaneous multi-spectral measurements by installing color filters within the plenoptic camera (see next section) [78,79], or derivation of physical quantities such as 3D flame temperature-fields by assuming proportionality between luminescence and temperature [80,81].

Similar to plenoptic-PIV, early works in plenoptic scalar-field measurements only achieved qualitative 3D reconstruction by refocusing the scene to create a focal-stack, and subsequently applying image segmentation to localize a subject in z. Subsequently, quantitative reconstructions were achieved by adopting a similar tomographic workflow as plenoptic-PIV, with the critical difference that the subject is no longer sparse particles. This has the immediate ramification that large scalar-field objects create proportionately giant zones of ambiguity. Consider a uniform-intensity spherical object imaged by just one camera ("Camera 2") in Fig. 13. The two red fans of rays define the side-most edges of the objects that Camera 2 sees, and their associated captured rays. The shaded region between the fans contain the object's zone of ambiguity, within which the plenoptic camera cannot distinguish between the presence or absence of object. Hence, a naïve

IOP Publishing Measurement Science and Technology
Journal **XX** (XXXX) XXXXXX https://doi.org/XXXX/XXXX

tomographic reconstruction will fill the shaded region.

Thus, complex scalar-fields are not easily resolved in spite of the plenoptic camera's perspective-view redundancy. This problem relates to the principle of limited-angle tomography, which stipulates that not all perspective-views are created equal [82]. For a given number of perspectives, views that are spaced far apart contribute significantly more quality to reconstruction than views of limited angles. Present research work around this issue by implementing multiple plenoptic cameras (or a camera with split view) to increase the effective measurement angle. I.e. as illustrated in Fig. 13, the zone of ambiguity is significantly reduced by adding just a second camera- though the resulting shape would still be far from smooth. The exact equivalence between the number of regular cameras versus plenoptic cameras required for scalar-field measurement remains to be determined.

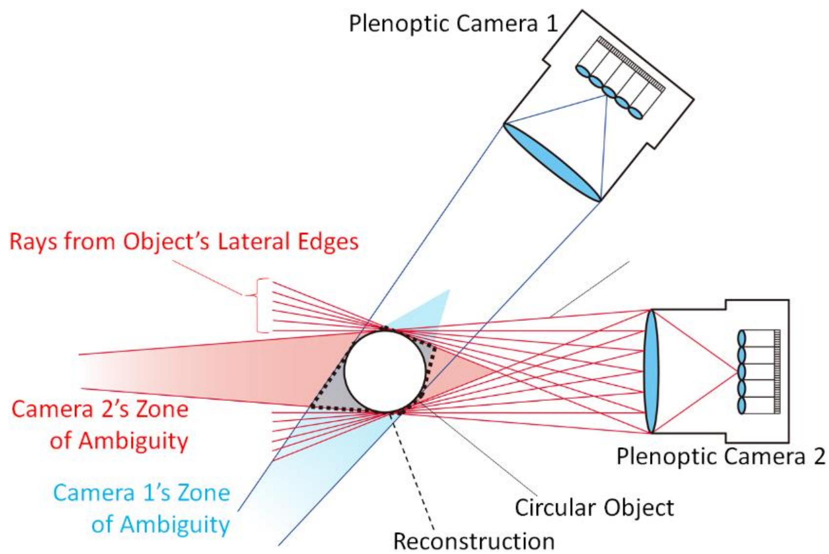

Fig. 13 The configuration and challenges of plenoptic 3D scalar-field measurement. Colored zones represent the zones of ambiguity for each camera. Whereas, the dotted diamond represents the combined zone of ambiguity for two cameras.

Some existing examples of plenoptic scalar-field measurements are shown in Fig. 14. Fig. 14A by Fischer et al. [29] represents an early unique application, where laser-scattering signals were elicited from two *planes* within a spray. The images resembled a smooth scalar-field due to sub-pixel droplet sizes. Fischer et al. then used refocusing to localize signals from both planes, after which the refocused images were interpreted through frequency modulation Doppler global velocimetry (FM-DGV) to determine each plane's droplets velocities. Fig. 14B by George et al. [79] describes a combustion experiment with two plenoptic cameras. A filtered variant of the focal-stack method was used for reconstruction. In addition to flame luminescence, George et al. was able to derive 3D distributions of soot loading, temperature and other quantities by filtering the cameras' wavelengths. Filtered focal-stack was ultimately concluded as insufficient and tomography recommended for future reconstructions. Fig. 14C also shows a scalar-field/flame study. This work by Liu et al. [76] compared the effects of camera number and three algorithms (namely, Algebraic Reconstruction Technique, ART; MART; and Maximum Likelihood Expectation Maximization, MLEM) on reconstruction quality. Both simulation and experimental data were employed. They confirmed that a single plenoptic camera was insufficient for 3D scalar-field measurement, and additionally concluded that MART was unsuitable for non-sparse scalar-fields. ART and MLEM performed similarly. In conclusion, Liu et al. also demonstrated improved results using a single Lytro plenoptic 1.0 camera modified with a three-view splitter for added parallax angle.

IOP Publishing
Measurement Science and Technology
Journal XX (XXXX) XXXXXX
https://doi.org/XXXX/XXXX

Ongoing works in this field continue to explore variations of algorithms to improve reconstruction, including adaptive simultaneous algebraic reconstruction technique (ASART) with total variation (TV) regularization [78], dynamic masking [78], and potential incorporation of prior knowledge among others. In our opinion, plenoptic cameras may not maximally demonstrate its potential in single-physics 3D scalar-field measurement, where large perspective-view redundancy does not equate to significant quality improvement. I.e. while a plenoptic approach may still lead to a reduction in the number of cameras, the reduction will not be proportional to the number of perspective-views per camera. Instead, a plenoptic camera may show its true advantage when employed in future multi-physics measurements such as combined 3D and multispectral measurement, where portions of the redundant perspective-views are devoted to sampling different physics. The groundwork for incorporating more physics into plenoptic flow diagnostics is touched upon in the section on plenoptic spectroscopic imaging.

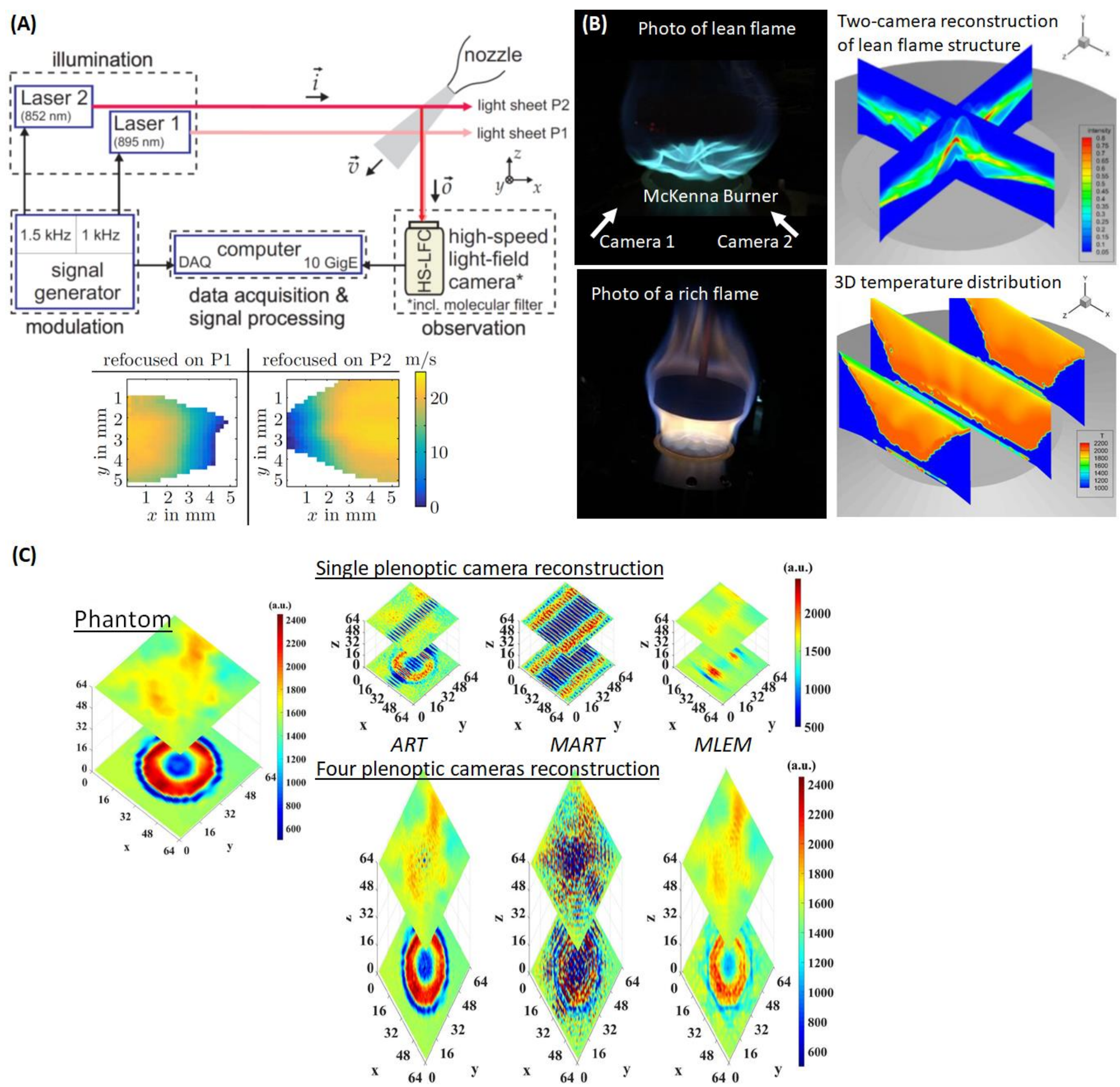

Fig. 14 Examples of plenoptic scalar-field measurements: (A) High-speed multi-plane frequency modulation Doppler global velocimetry (FM-DGV) by [29]. (B) 3D reconstruction of flame structure, temperature-field and other quantities through filtered-refocusing and two plenoptic cameras [79]. (C) [76]'s assessment of the effects of algorithm and camera number on reconstruction quality.

IOP Publishing Measurement Science and Technology
Journal **XX** (XXXX) XXXXXX https://doi.org/XXXX/XXXX

7. Application to Background-Oriented Schlieren (BOS)

BOS is a prevalent technique in flow diagnostics, especially for studying supersonic aerodynamics and mixture interfaces, due to its simplicity and non-intrusiveness, where only a patterned background is required to determine density gradients around a subject. However, similar to scalar-field tomography, the camera apparatus to acquire 3D BOS measurements is cumbersome [83] and plenoptic-BOS [84–88] represents a potential for cost and complexity reduction. Like plenoptic-PIV, plenoptic-PTV and scalar-field measurement, early plenoptic-BOS efforts employed focal-stack for qualitative 3D localization [85,86]. The associated workflow is illustrated on the top-half of Fig. 15: two separate plenoptic images are first taken, with and without distortion of the patterned background. Subsequently, these images are decoded into perspective-views. Cross-correlation between the two sets of perspective-views provide 2D background displacement field in each perspective. From these "displacement perspectives," a refocusing procedure that treats displacements as equivalent intensities is implemented to create a BOS focal-stack. An example of such a stack is shown in Fig. 16A for two stings at different depths in a supersonic flow, Sting B at around $z \approx -20mm$ and Sting A at $z \approx 4mm$. Color represents displacement magnitude. It is evident that displacement features appear sharpest when the BOS image is refocused to their corresponding depth. Thus, a low resolution 3D localization can be achieved based on image sharpness in the focal-stack.

More recent plenoptic-BOS studies attempt to acquire higher resolution 3D reconstruction of density field by adopting the tomographic approach [88]. As shown in the bottom-half of Fig. 15, the displacement perspectives are processed through a tomographic reconstruction routine much alike scalar-field reconstruction in this approach. Consequently, a 3D displacement-field is generated, from which 3D density-field can be acquired. This tomographic approach suffers from the same challenges as scalar-field tomography, where the field is too information-rich for a single plenoptic camera's limited parallax angle. The effect is exhibited in Fig. 16B of an experiment with two translucent cylinders immersed in *nearly* index-matched liquid, and four plenoptic cameras. Reconstruction with only two cameras resulted in rough diamond-shapes objects. The incorporation of a third camera substantially rounded the reconstructed objects, making them closer to the ground truth (dotted circles). Summarily, as they face similar challenges, we expect development in plenoptic scalar-field measurement and BOS to be parallel and mutually beneficial in the near future.

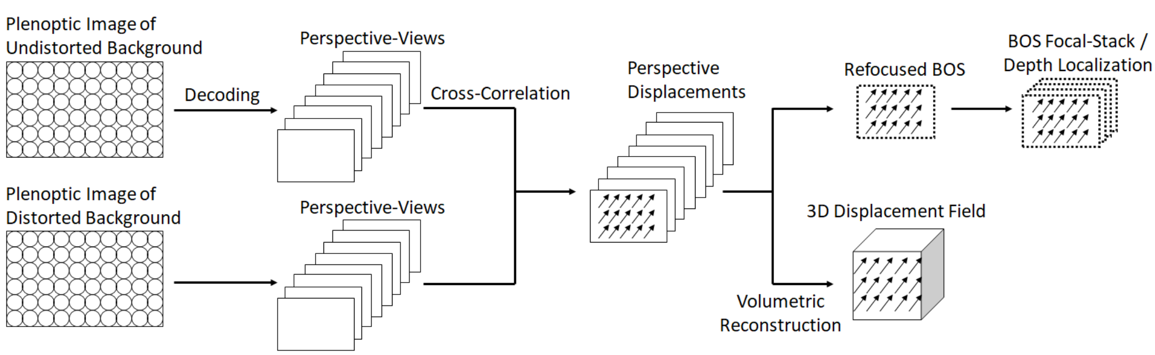

Fig. 15 Two plenoptic-BOS work-flows: refocusing (top) and tomography (bottom).

IOP Publishing
Measurement Science and Technology
Journal **XX** (XXXX) XXXXXX
https://doi.org/XXXX/XXXX

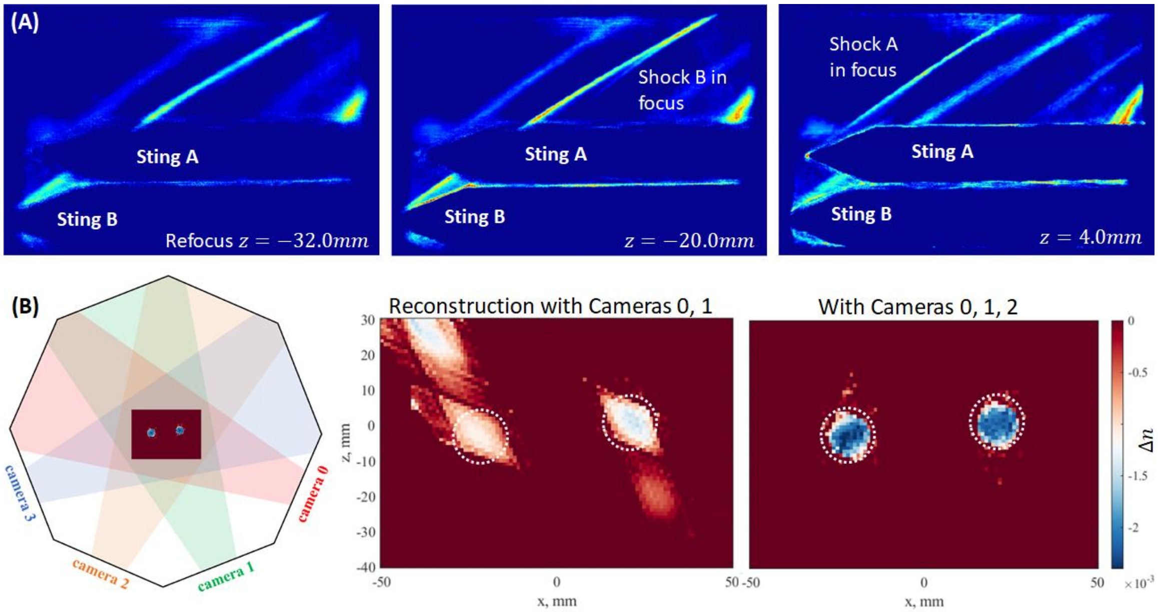

Fig. 16 Examples of plenoptic-BOS in (A) qualitative 3D localization two stings' shockwaves as part of Klemkowsky et al.'s developmental work [85,86] and (B) quantitative tomographic reconstruction [88].

8. Application to Spectroscopic Imaging

While previous applications of plenoptic camera have focused on multiplexing numerous perspectives onto a single sensor, a recent line of research proposed wavelength-multiplexing. As shown in Fig. 17, the fundamental architecture involves a plenoptic 1.0 system, which conveniently decouples (s,t) and (u,v). A color filter is ideally placed at the main-lens' aperture plane where (u,v) is mapped, such that rays from an object are filtered by wavelengths λ depending on their incident angles. I.e. λ is mapped to (u,v). And, since (u,v) is two dimensional, a color filter with 2D pattern can be used. The result of this mapping is shown on the (s,t) vs. (u,v) sampling diagram on the right of Fig. 17, where images of specific λ can be rendered identically as perspective-views. Notably, this approach only works on objects within the DOF of the nominal focal-plane, since objects away from the focal-plane will defocus and spread across multiple microlens, losing its direct (u,v) multiplexing pattern.

Key works in this area include [89–91], which separately used discrete and continuous color filters to gain spectral information of a scene. In both cases, the spectral information is further mapped against a blackbody distribution to gain insights into a scene's temperature, in a manner more precise than single-wavelength infrared thermometry. Used for spectroscopy, plenoptic multi-band imaging would also compare favorably against traditional point-measurement spectroscopes, against imagers that separate wavelengths by prisms/dichroic-mirrors and requires one camera per wavelength, or the use of filter wheels that compromise the time-resolved capability of the sensor, or against wavelength-filtering on the sensor's Bayer filter, which is not currently amenable to customization from a cost standpoint.

Multi-band plenoptic imaging is only in its infancy, and while valuable on its own, we see the next step in development as extending the multi-band imaging capability to 3D. Breaking the limitation of confining objects to the DOF will offer greater potential in adopting it as a doorway to more complex measurements such as combined multi-spectral scalar-field tomography or FSI measurements where surface and flow tracers are filtered by wavelength, as well as a doorway to rendering colors on otherwise monochromatic devices such as night-vision image intensifier.

IOP Publishing Measurement Science and Technology
Journal **XX** (XXXX) XXXXXX https://doi.org/XXXX/XXXX

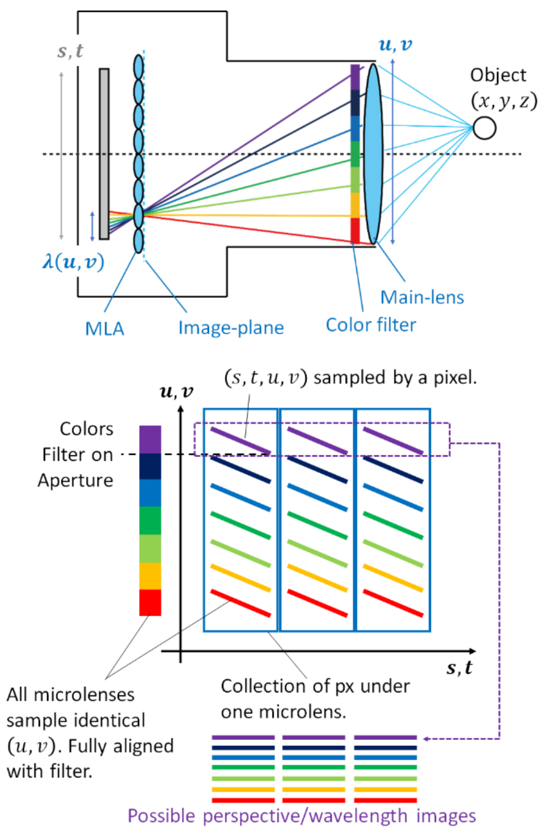

Fig. 17 Principles of plenoptic spectroscopic imaging.

9. Future

The future of plenoptic flow diagnostics will benefit from both evolutionary hardware improvements as well as revolutionary architectural shifts. Evolution in image sensors will progressively allow for experiments with faster temporal dynamics, where currently ~1000*fps* is near the upper limit due to plenoptic cameras' resolution requirement. Evolution in MLA fabrication will continue to enable cheaper and more precise devices - as well as more creative implementations such as the heterogeneous focal-length MLA [92]. At present, a large percentage of plenoptic flow diagnostics rely on the 1.0 architecture and its conveniently decoupled (s, t) and (u, v) data. A migration to plenoptic 2.0, especially with the ability to control $(s, t) : (u, v)$ trade-off on-the-fly will alleviate the resolution demand of plenoptic systems and possibly redefine the cost and capability of many plenoptic techniques. Finally, projecting further into the future, the advent of more powerful smartphone sensors will eventually see migration of some users from large-sensor plenoptic camera to camera-array LF imaging based on small, cheap sensors- possibly in highly decentralized configurations optimized to particular experiments.

On the software side, the decoding of perspective-views from a raw image is the first step in most plenoptic techniques. Presently, decoded images suffer from low resolution, low SNR and interpolation artifacts that limit the range of data processing one can performed on perspective-views. Research in super-resolution, AI-driven data enhancement and refinement in decoding techniques will continue to improve image quality for a given hardware for some time to come. Outside of decoding, new calibration algorithms including higher-order corrections and auto-calibration will continue to improve 3D results and workflow ergonomics. Meanwhile, more advanced regularizations and tomography algorithms will improve and accelerate 3D reconstruction. Outside of predictable developments, we expect novel cross-disciplinary techniques to arise from rapid progress in the machine vision community, which has also taken interests in plenoptic and LF imaging. Finally, design and operation of these cameras still presently require significant experience and expertise. The simplification of plenoptic techniques into plug-and-play systems remain an industrial design challenge to be tackled both on hardware and software fronts.

Though exciting advancements are on the horizon, the challenge of limited parallax baseline and spatial-angular resolution tradeoff remain fundamental to plenoptic systems. Thus, for 3D applications where conventional approaches will suffice, plenoptic cameras provide some simplification and cost-saving, but not necessarily a transformative new capability. Instead, the biggest future value of plenoptic flow diagnostics may lie in its ability to fuse different diagnostics within one sensor, allowing it to achieve many conventionally impossible or impractical experiments. One early example is the fusion of plenoptic-PIV and 3D tracking under one camera to achieve 3D FSI measurement [93,94], as shown in Fig. 18. In this case, the equivalent conventional approach involves simultaneously exercising tomo-PIV and stereo-digital image correlation, which would have required six cameras, rendering the experiment prohibitive in cost and complexity [2,3]. Numerous other configurations of plenoptic diagnostics fusion remain to be explored in the near future.

IOP Publishing Measurement Science and Technology
Journal **XX** (XXXX) XXXXXX https://doi.org/XXXX/XXXX

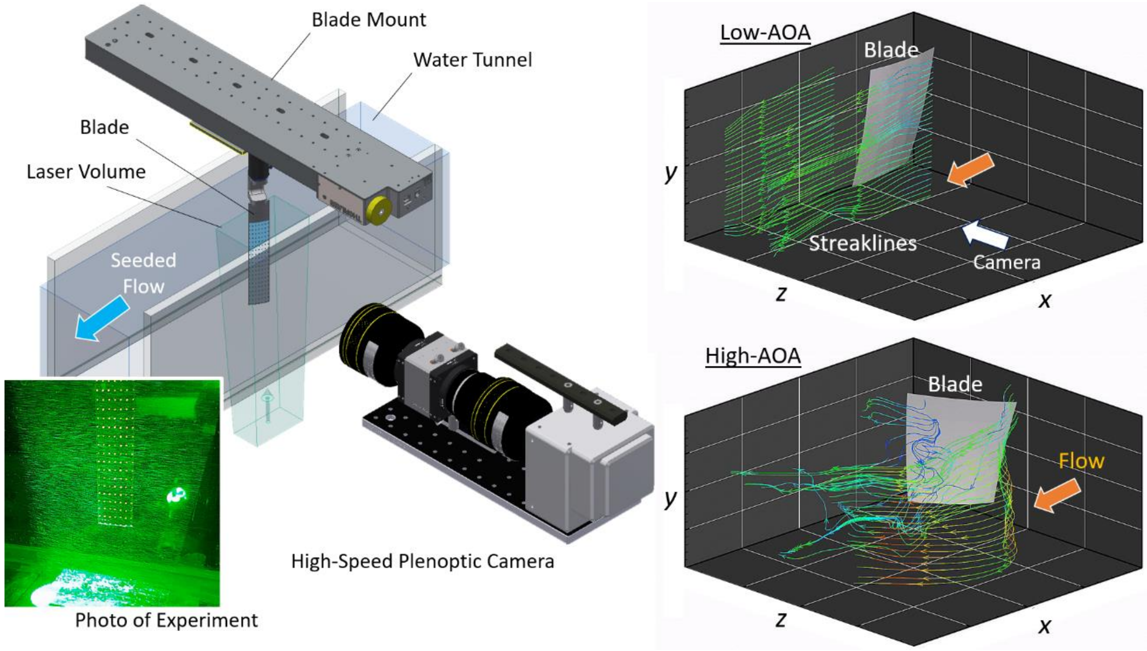

Fig. 18 Example of plenoptic diagnostics-fusion: single-camera FSI measurement performed by the author's group. Figure shows simultaneous 3D tracking of a blade with 2.5cm chord and 3D velocimetry of its associated flow-field at different angles of attack (AOA). Tracking is based on surface markers while velocimetry is based on flow seeding. [93,94]

Acknowledgements

The authors are grateful for several sources of support that were instrumental in much of the work discussed here including the Air Force Office of Scientific Research, the National Science Foundation, NASA Langley, Sandia National Laboratories and the Army Research Office. The authors are also grateful for the National Science Foundation's Major Research Instrumentation Program Grant No. 1725929 and Taiwan's Ministry of Science and Technology MOST 109-2222-E-009-012-MY3 that supported the writing of this article.

References

[1] Scarano F 2013 Tomographic PIV: Principles and practice *Meas. Sci. Technol.* **24** 012001
[2] Phillips N Fluid-Structure Interaction Studies on Bioscience Subjects *LaVision Focus Imaging*
[3] Acher G, Thomas L, Tremblais B, Gomit G, Chatellier L and David L 2019 *13th International Symposium on Particle Image Velocimetry*
[4] Zhou B, Li T, Frank J H, Dreizler A and Böhm B 2020 Simultaneous 10 kHz three-dimensional CH2O and tomographic PIV measurements in a lifted partially-premixed jet flame *Proc. Combust. Inst.* **000** 1–9
[5] Ebi D and Clemens N T 2016 Simultaneous high-speed 3D flame front detection and tomographic PIV *Meas. Sci. Technol.* **27** 035303
[6] Halls B R, Hsu P S, Jiang N, Legge E S, Felver J J, Slipchenko M N, Roy S, Meyer T R and Gord J R 2017 kHz-rate four-dimensional fluorescence tomography using an ultraviolet-tunable narrowband burst-mode optical parametric oscillator *Optica* **4** 897
[7] Kim J T, Kim D, Liberzon A and Chamorro L P 2016 Three-dimensional particle tracking velocimetry for turbulence applications: case of a jet flow *J. Vis. Exp.* **108** 53745
[8] Kang M W, Wu Y and Ma L 2014 Fiber-based endoscopes for 3D combustion measurements: view registration and spatial resolution *Combust. Flame* **161** 3063–72
[9] MiniShaker *LaVision* https://www.lavision.de/en/download.php?id=3333
[10] Jux C, Sciacchitano A, Schneiders J F G and Scarano F 2018 Robotic volumetric PIV of a full-scale cyclist *Exp. Fluids* **59** 1–15

IOP Publishing Measurement Science and Technology

Journal **XX** (XXXX) XXXXXX https://doi.org/XXXX/XXXX

[11] Pereira F and Gharib M 2002 Defocusing digital particle image velocimetry and the three-dimensional characterization of two-phase flows *Meas. Sci. Technol.* **13** 683–94

[12] Malek M, Allano D, Coëtmellec S, Özkul C and Lebrun D 2004 Digital in-line holography for three-dimensional-two-components particle tracking velocimetry *Meas. Sci. Technol.* **15** 699–705

[13] Pick S and Lehmann F O 2009 Stereoscopic PIV on multiple color-coded light sheets and its application to axial flow in flapping robotic insect wings *Exp. Fluids* **47** 1009–23

[14] Adelson E H and Wang J Y A 1992 Single Lens Stereo with a Plenoptic Camera *IEEE Trans. Pattern Anal. Mach. Intell.* **14**

[15] Ng R, Levoy M, Bredif M, Duval G, Horowitz M and Hanrahan P 2005 Light field photography with a hand-held plenoptic camera *Stanford University Computer Science Tech Report CSTR*

[16] Lumsdaine A and Georgiev T 2010 The focused plenoptic camera plenoptic camera *IEEE International Conference on Computational Photography*

[17] Georgiev T and Lumsdaine A 2010 Reducing plenoptic camera artifacts *Comput. Graph. Forum* **29** 1955–68

[18] Johannsen O, Heinze C, Goldluecke B and Perwaß C 2013 On the calibration of focused plenoptic cameras. In: Grzegorzek M, Theobalt C, Koch R, Kolb A (eds) *Time-of-Flight and Depth Imaging. Sensors, Algorithms, and Applications. Lecture Notes in Computer Science* **8200**

[19] Strobl K H and Lingenauber M 2016 Stepwise calibration of focused plenoptic cameras *Comput. Vis. Image Underst.* **145** 140–7

[20] Hog M, Sabater N, Vandame B and Drazic V 2017 An image rendering pipeline for focused plenoptic cameras *IEEE Trans. Comput. Imaging* **3** 811–21

[21] Hadfield J and Nobes D S 2016 *18th International Symposium on the Application of Laser and Imaging Techniques to Fluid Mechanics*

[22] Ihrke I, Restrepo J and Mignard-Debise L 2016 Principles of light field imaging: briefly revisiting 25 years of research *IEEE Signal Process. Mag.* **33** 59–69

[23] Cho D, Lee M, Kim S and Tai Y W 2013 *IEEE International Conference on Computer Vision (ICCV)*

[24] Raytrix 2002 3D Light-field plenoptic cameras https://raytrix.de/products

[25] Liu Y, Hossain M, Sun J, Xu C, Zhang B and Wang S 2017 *IEEE SENSORS*

[26] Tan Z P, Johnson K, Clifford C and Thurow B S 2019 Development of a modular, high-speed plenoptic-camera for 3D flow-measurement *Opt. Express* **27** 13400

[27] Tan Z P and Thurow B S 2020 Depth-of-field reduction due to blurring in a relayed plenoptic camera and mitigation via deconvolution *Meas. Sci. Technol.* **31** 055403

[28] Dansereau D G, Schuster G, Ford J and Wetzstein G 2017 *30th IEEE Conference on Computer Vision and Pattern Recognition*

[29] Fischer A, Kupsch C, Gürtler J and Czarske J 2015 High-speed light field camera and frequency division multiplexing for fast multi-plane velocity measurements *Opt. Express* **23** 24910

[30] Song X, Gu M, Cao L, Tang Z and Xu C 2019 A microparticle image velocimetry based on light field imaging *IEEE Sens. J.* **19** 9806–17

[31] Georgiev T and Lumsdaine A 2009 Super resolution with plenoptic camera 2.0 *Adobe Syst. Inc. Tech. Rep* 1–9

[32] Belden J, Truscott T T, Axiak M C and Techet A H 2010 Three-dimensional synthetic aperture particle image velocimetry *Meas. Sci. Technol.* **21** 125403

[33] Sakr S 2013 Pelican imaging's 16-lens array camera coming to smartphone next year *Engadget*

[34] Locklear M 2018 Light's multi-lens camera tech is coming to a phone *Engadget*

[35] Tan Z P, Alarcon R, Allen J, Thurow B S and Moss A 2020 Development of a high-speed plenoptic imaging system and its application to marine biology PIV *Meas. Sci. Technol.* **31** 054005

[36] Xu S, Mei D, Ding J, Shi S, Li H, Liu Y and Jiang B 2019 *13th International Symposium on Particle Image Velocimetry*

[37] Wabick K J, Berdon R L, Buchholz J H J, Johnson K C and Thurow B S 2018 *AIAA SciTech Forum*

[38] Johnson K C, Thurow B S, Kim T, Blois G and Christensen K T 2016 *18th International Symposium on Applications of Laser and Imaging Techniques to Fluid Mechanics*

[39] Bolton J T, Thurow B, Aroraz N and Alvix F S 2016 *32nd AIAA Aerodynamic Measurement Technology, Ground Testing, and Flight Testing Conference*

[40] Jones C, Bolton J, Clifford C, Thurow B, Arora N and Alvi F 2020 Single-camera three-dimensional velocity measurement of a fin-generated shock-wave/boundary-layer interaction *AIAA J.* **58** 4438–50

[41] Kvon A, Kharlamov S and Bobylev A 2019 *13th International Symposium on Particle Image Velocimetry*

[42] Gururaj A, Moaven M, Tan Z P, Thurow B and Raghav V 2020 *AIAA Scitech Forum*

IOP Publishing Measurement Science and Technology
Journal **XX** (XXXX) XXXXXX https://doi.org/XXXX/XXXX

[43] Raghav V, Clifford C, Midha P, Okafor I, Thurow B and Yoganathan A 2019 Three-dimensional extent of flow stagnation in transcatheter heart valves *J. R. Soc. Interface* **16** 20190063
[44] Lynch K 2011 *MSc Thesis* Auburn University
[45] Fahringer T W, Lynch K P and Thurow B S 2015 Volumetric particle image velocimetry with a single plenoptic camera *Meas. Sci. Technol.* **26** 115201
[46] Fahringer T W and Thurow B S 2012 *42nd AIAA Fluid Dynamics Conference*
[47] Kawaguchi T, Saito T and Satoh I 2014 *17th International Symposium Applications of Laser and Imaging Techniques to Fluid Mechanics*
[48] Shi S, Ding J, New T H and Soria J 2017 Light-field camera-based 3D volumetric particle image velocimetry with dense ray tracing reconstruction technique *Exp. Fluids* **58** 78
[49] Fahringer T and Thurow B 2015 *11th Intertional Symposium on Particle Image Velocimetry*
[50] Anglin P, Reeves S J and Thurow B S 2017 Characterization of plenoptic imaging systems and efficient volumetric estimation from plenoptic data *IEEE J. Sel. Top. Signal Process.* **11** 1020–33
[51] Cao L, Zhang B, Hossain M M, Li J and Xu C 2020 Tomographic reconstruction of light field PIV based on backward ray-tracing technique *Meas. Sci. Technol.* **32** 044007
[52] Thomason C M, Fahringer T F and Thurow B S 2014 *52nd AIAA Aerospace Sciences Meeting*
[53] Hall E M, Fahringer T W, Thurow B S and Guildenbecher D R 2017 *55th AIAA Aerospace Sciences Meeting*
[54] Hall E M, Fahringer T W, Guildenbecher D R and Thurow B S 2018 Volumetric calibration of a plenoptic camera *Appl. Opt.* **57** 914
[55] Shi S, Ding J, New T H, Liu Y and Zhang H 2019 Volumetric calibration enhancements for single-camera light-field PIV *Exp. Fluids* **60** 1–16
[56] Zhao Y, Li H, Mei D and Shi S 2020 Metric calibration of unfocused plenoptic cameras for three-dimensional shape measurement *Opt. Eng.* **59** 1
[57] Wieneke B 2008 Volume self-calibration for 3D particle image velocimetry *Exp. Fluids* **45** 549–56
[58] Fahringer T 2018 *PhD Dissertation* Auburn University
[59] Deem E A, Zhang Y, Cattafesta L N, Fahringer T W and Thurow B S 2016 On the resolution of plenoptic PIV *Meas. Sci. Technol.* **27** 084003
[60] Shekhar C, Ogawa S and Kawaguchi T 2017 Feasibility and accuracy assessment of light field (plenoptic) PIV flow-measurement technique *EPJ Web Conf.* **143** 02102
[61] Rice B E, McKenzie J A, Peltier S J, Combs C S, Clifford C and Thurow B 2018 *56th AIAA Aerospace Sciences Meeting*
[62] Fahringer T W and Thurow B S 2018 Plenoptic particle image velocimetry with multiple plenoptic cameras *Meas. Sci. Technol.* **29** 075202
[63] La Foy R R and Vlachos P 2013 *10th International Symposium on Particle Image Velocimetry*
[64] Eckstein A and Vlachos P P 2009 Digital particle image velocimetry (DPIV) robust phase correlation *Meas. Sci. Technol.* **20** 055401
[65] Hall E M, Guildenbecher D R and Thurow B S 2017 Uncertainty characterization of particle location from refocused plenoptic images *Opt. Express* **25** 21801
[66] Nobes D S, Chatterjee O and Setayeshgar A 2014 *17th International Symposium on Applications of Laser and Imaging Techniques to Fluid Mechanics*
[67] Hall E M 2019 *PhD Dissertation* Auburn University
[68] Hadfield J 2018 *MSc Thesis* University of Alberta
[69] Clifford C, Tan Z P, Hall E and Thurow B 2019 *13th International Symposium on Particle Image Velocimetry*
[70] Wagner N, Norlin N, Gierten J, deMedeiros G, Balázs B, Wittbrodt J, Hufnagel L and Prevedel R 2019 Instantaneous isotropic volumetric imaging of fast biological processes *Nature Methods* **16** 497-500
[71] Broxton M, Grosenick L, Yang S, Cohen N, Andalman A, Deisseroth K and Levoy M 2013 Wave optics theory and 3-D deconvolution for the light field microscope *Opt. Express* **21** 25418
[72] Levoy M, Ng R, Adams A, Footer M and Horowitz M 2006 Light field microscopy *ACM Trans. Graph.* **25** 924–34
[73] Levoy M, Zhang Z and McDowall I 2009 Recording and controlling the 4D light field in a microscope using microlens arrays *J. Microsc.* **235** 144–62
[74] Truscott T T, Belden J, Ni R, Pendlebury J and McEwen B 2017 Three-dimensional microscopic light field particle image velocimetry *Exp. Fluids* **58** 1–14
[75] Truong T V, Holland D B, Madaan S, Andreev A, Keomanee-Dizon K, Troll J V, Koo D E S, McFall-Ngai M J and Fraser S E 2020 High-contrast, synchronous volumetric imaging with selective volume illumination microscopy *Communications Biology* **3** 74
[76] Liu H, Wang Q and Cai W 2019 Assessment of plenoptic imaging for reconstruction of 3D discrete and continuous luminous fields *J. Opt. Soc. Am. A* **36** 149

IOP Publishing Measurement Science and Technology
Journal **XX** (XXXX) XXXXXX https://doi.org/XXXX/XXXX

[77] Li T J, Sun J, Yuan Y, Xu C L, Shuai Y and Tan H P 2018 Simulation of calibration process in flame measurement by plenoptic camera *Appl. Therm. Eng.* **135** 179–87

[78] Clifford C J and Thurow B S 2020 On the impact of subaperture sampling for multispectral scalar field measurements *Optics* **1** 136–54

[79] George J, Clifford C, Jenkins T P and Thurow B S 2019 Volumetric spectral imaging and two-color pyrometry of flames using plenoptic cameras *Applied Optical Metrology* **III** 1110216

[80] Huang X, Qi H, Zhang X L, Ren Y T, Ruan L M and Tan H P 2018 Application of Landweber method for three-dimensional temperature field reconstruction based on the light-field imaging technique *J. Heat Transfer* **140** 1–11

[81] Sun J, Hossain M M, Xu C and Zhang B 2018 Investigation of flame radiation sampling and temperature measurement through light field camera *Int. J. Heat Mass Transf.* **121** 1281–96

[82] Delaney A H and Bresler Y 1998 Globally convergent edge-preserving regularized reconstruction: an application to limited-angle tomography *IEEE Trans. Image Process.* **7** 204–21

[83] Schwarz A 1996 Multi-tomographic flame analysis with a schlieren apparatus *Meas. Sci. Technol.* **7** 406

[84] Bichal A 2015 *PhD Dissertation* Auburn University

[85] Klemkowsky J, Thurow B and Mejia-Alvarez R 2016 *54th AIAA Aerospace Sciences Meeting*

[86] Klemkowsky J N, Fahringer T W, Clifford C J, Bathel B F and Thurow B S 2017 Plenoptic background oriented schlieren imaging *Meas. Sci. Technol.* **28** 095404

[87] Klemkowsky J N, Clifford C J, Bathel B F and Thurow B S 2019 A direct comparison between conventional and plenoptic background oriented schlieren imaging *Meas. Sci. Technol.* **30** 064001

[88] Davis J K 2020 *PhD Dissertation* Auburn University

[89] Danehy P M, Hutchins W D, Fahringer T and Thurow B S 2017 *55th AIAA Aerospace Sciences Meeting*

[90] Fahringer T W, Danehy P M and Hutchins W D 2018 *AIAA Aviation Forum*

[91] Kelly D L, Phillips M A, Thurow B S and Scarborough D E 2020 *AIAA Scitech 2020 Forum*

[92] Perwaß C and Wietzke L 2012 Single lens 3D-camera with extended depth-of-field *Human Vision and Electronic Imaging* **XVII** 829108

[93] Thurow B, Tan Z P, Tiwari B and Raghav V 2019 *72nd Annual Meeting of the APS Division of Fluid Dynamics*

[94] Thurow B, Raghav V and Tan Z P 2020 *73rd Annual Meeting of the APS Division of Fluid Dynamics*